JPE 18-6-21

https://doi.org/10.6113/JPE.2018.18.6.1844
ISSN(Print): 1598-2092 / ISSN(Online): 2093-4718

Stability Control of Energy Storage Voltage Source Inverters in Isolated Power Systems

Jian Hu† and Lijun Fu*

†,*National Key Laboratory of Science and Technology on Vessel Integrated Power System, Naval University of Engineering, Wuhan, China

Abstract

Isolated power systems (IPS) are often characterized by a weak grid due to small power grids. The grid side voltage is no longer equivalent to an ideal voltage source of an infinitely big power grid. The conversion control of new energy sources, parameter perturbations as well as the load itself can easily cause the system voltage to oscillate or to become unstable. To solve this problem, increasing the energy-storage power sources is usually used to improve the reliability of a system. In order to provide support for the voltage, the energy-storage power source inverter needs an method to control the voltage source. Therefore, this paper has proposed the active damping control of a voltage source inverter (VSI) based on virtual compensation. By simplifying the VSI double closed-loop control, two feedback compensation channels have been constructed to reduce the VSI output impedance without changing the characteristics of the voltage gain of a system. This improvement allows systems to operate stably in a larger range. A frequency-domain analysis, and simulation and experimental results demonstrate the feasibility and effectiveness of the proposed method.

Key words: Active damping, Double closed-loop control, Energy-storage power sources, Stability, Voltage source inverter

I. INTRODUCTION

With the development of isolated power systems (IPSs), they have been widely used in ships and automobiles as well as in remote areas like islands and deserts due to their flexible power-generation and simple network structure. IPSs are smaller in scale than ground interconnected grid systems and its ratio of short-circuit capacity to power generation capacity is relatively low. Therefore, the IPS has the characteristic of a weak-grid. In this case, its grid-side voltage is not equivalent to the ideal voltage source of an infinitely big power grid. Changes in the source side and in the load side cause fluctuations of the system voltage. There are many forms of energy in IPSs that need to be unified and transformed by various converters. The impedance matching of cascade-connected power electronic devices has a direct influence on the system voltage stability.

Manuscript received Apr. 28, 2018; accepted Jul. 15, 2018
Recommended for publication by Associate Editor Kai Sun.
†Corresponding Author: hujian0113@qq.com
Tel: +86-13098883659, Naval University of Engineering
*National Key Laboratory of Science and Technology on Vessel Integrated Power System, Naval University of Engineering, China

An extensive study is conducted to improve the voltage stability of an inverter running with a load and to solve the problems of voltage waveform distortion and oscillation of the inverter under a weak grid. The authors of [1] and [2], applied inverter reactive power control and proposed a voltage regulation strategy based on the reactive power of a photovoltaic inverter to ensure that the voltage of the inverter's grid point is within the normal operating range. However, in actual control, there may not be enough controllable reactive power. The authors of [3] analyzed the insufficiency of the reactive power of a current source inverter whose control characteristics are greatly affected by network impedance under the condition of a weak grid. In addition, a voltage feedforward control and a phase advance compensation were employed to stabilize the system. The authors of [4] presented an improved capacitive current feedback control that allows the stability limited range of the resonant frequency to extend from a sixth of a sampling frequency to a quarter. The authors of [5] proposed an active damping control method based on the point of common coupling voltage feedback to reduce the instability of an inverter caused by a wide-range change in the load impedance under a weak grid. The authors of [6] used an adaptive method

to adjust the active damping resistors according to the point of common coupling voltage to allow the output impedance of the system to stay at a stable critical value to reduce the losses. In [7], a full-state feedback equivalent active damping controller was designed to improve the stability and to reduce the number of sensors required in a system.

The above methods mentioned in [3]-[7] are intended for current source inverters. However, the energy storage serves as a voltage support in the IPS, and the inverter usually works in the mode of a voltage source. Based on [4], the authors of [8] proposed active damping control of the inductive current feedback of a VSI, which can broaden the resonance frequency range for the stability of an inverter. The authors of [9] put forward a positive feedback active damping control to deal with the stability of the cascade connection between the VSI and the subsystem. In [10], the adaptive control of voltage was applied to a VSI to obtain a faster system response and a zero static error. The authors of [11] offered a composite nonlinear feedback control of a VSI to improve the system transient and static performance. The authors of [12] presented the rapid control of a VSI based on an adaptive droop DC-bus voltage controller. However, it is only applicable to single-phase inverters. The authors of [13] provided current loop control for a VSI based on a robust PR controller to enhance the robustness of the system to parametric uncertainty.

In order to improve the stability of the output voltage of an energy storage VSI, and to broaden the stable operating range of the system, this paper proposes the active damping control of a VSI based on virtual compensation. For the sake of convenience, the five-closed-loop system is simplified to a three-closed-loop system by offsetting the voltage feedforward and physical feedback in the double closed-loop control of existing traditional VSIs. Then the small time-constant link is modified, and positive and negative feedback channels are added to the front and back of the PI controller in the current loop, in order to offset the sampling frequency link and to produce active damping. Finally, the proposed control is shown to be better than the existing conventional VSI double closed-loop control according to a frequency domain analysis, and simulation and experimental results. This can reduce the output impedance without changing the output characteristic so the load can have a wider range of impedance and the stability margin of the system can be improved.

II. Conventional VSI Double Closed-Loop Control

The conventional VSI control mainly uses the double closed-loop control [14], which is a composition of a current inner loop and a voltage outer loop. Usually, ac filter capacitor voltage is chosen as the feedback variable of the voltage outer loop and the ac filter inductance current is chosen as the feedback variable of the current inner loop.

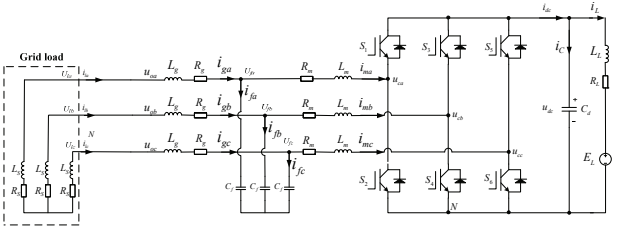

Fig. 1. Topological structure of a three-phase inverter.

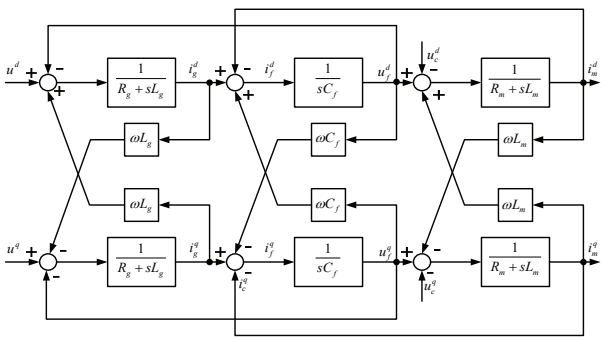

Fig. 2. Block diagram of the state model of an inverter in the synchronous coordinate system.

The main circuit topology of a three-phase inverter is shown in Fig. 1. R_g, L_g, R_m, L_m and C_f represent the inverter load-side equivalent resistance and leakage inductance, the inverter-side equivalent resistance, the inductance and the filter capacitance, respectively.

According to the state model of an inverter in the synchronous coordinate system, its block diagram is shown in Fig. 2.

From Fig. 2, it can be seen that the mutual coupling between the *dp* axial variables results in difficulty in designing the VSI controller. Therefore, it is necessary to decouple the inverter in the design. The use of an algorithm based on feedforward decoupling makes it possible for the inverter to perform decoupling control of the *dq* axis. The specific methods for doing so can be found in [14]. A block diagram of the VSI double closed-loop control is given in Fig. 3.

In Fig. 3, T_s is the sampling period, and K_{PWM} is the inverter PWM equivalent gain. For the per-unit system, $K_{\mathrm{PWM}}=V_{\mathrm{base}}$, K_{c} is the current sampling ratio and K_{v} is the voltage sampling ratio. The load current feedforward coefficient is determined as α, the capacitive voltage feedforward coefficient is determined as β, and $G_v(s)=K_{vP}+K_{vI}/s$ and $G_i(s)=K_{iP}+K_{iI}/s$ are determined as the voltage outer loop PI controller and the current inner loop PI controller, respectively.

The output voltage of the VSI can be expressed as:

$$v_f(s)=v_f^*H_1(s)-H_2(s)i_g \tag{1}$$

Where $H_1(s)$ is the transfer function of the output voltage relative to the reference gain, and $H_2(s)$ is the transfer function of the output voltage relative to the load current, namely the output impedance of the inverter. According to

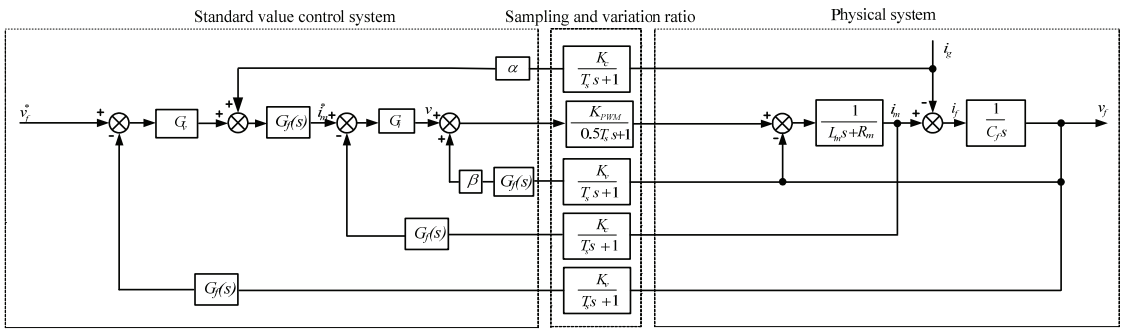

Fig. 3. Block diagram of the VSI double closed-loop control.

Fig. 3, they are expressed as:

$$H_1(s)=\frac{G_f(s)G_{vsi}(s)G_v(s)G_i(s)G_1(s)G_2(s)}{\Delta(s)} \tag{2}$$

$$\begin{aligned}H_2(s)=&\frac{G_2(s)(1+G_i(s)G_{vsi}(s)G_1(s)H_c(s)G_f(s))}{\Delta(s)}\\&-\frac{\alpha H_c(s)G_f(s)G_{vsi}(s)G_i(s)G_1(s)G_2(s)}{\Delta(s)}\end{aligned} \tag{3}$$

$$\begin{aligned}\Delta(s)=&1+G_1(s)G_2(s)-\beta G_f(s)H_v(s)G_{vsi}(s)G_1(s)G_2(s)\\&+G_f(s)H_c(s)G_{vsi}(s)G_1(s)G_i(s)\\&+G_f^2(s)H_v(s)G_{vsi}(s)G_v(s)G_i(s)G_1(s)G_2(s)\end{aligned} \tag{4}$$

Where $H_v(s)=K_v/(T_s s+1)$, $H_c(s)=K_c/(T_s s+1)$ and $G_{vsi}(s)=K_{PWM}/(0.5T_s s+1)$ are delays introduced by the digital control system. In addition, $G_f(s)=\omega_f/(s+\omega_f)$ is the digital low-pass filter used in the actual digital controller, the parameter ω_f of the low-pass filter represents the filtering angular frequency, $\omega_f=2\pi f$, f=50Hz. Therefore, $\omega_f=100\pi$; $G_1(s)=1/(L_m s+R_m)$; $G_2(s)=1/C_f s$; $G_3(s)=(L_g s+R_g)$; $K_v=1/V_{base}$; and $K_c=1/I_{base}$.

III. VSI Active Damping Control Based on Virtual Compensation

A. Simplification of the Double Closed-Loop Control System by Offset

According to the block diagram of an actual controller shown in Fig. 3, in addition to considering the mathematical model of the inverter, there is a need to consider the double closed-loop control model which is too complex due to the capacitor voltage feedforward link $\beta G_f(s)H_v(s)$ and the inductor current feedforward link $\alpha H_v(s)$. The control model involves five closed-loops. For the design of the double closed-loop of the system, the amount of calculation is too big for analysis.

The rational design of the coefficients α and β helps to simplify the double closed-loop control of the VSI. Without consideration of the current loop, the equivalent control of the capacitor voltage feedforward system is shown in Fig. 4.

In Fig. 4, before the capacitor voltage feedforward and actual physical feedback offset, the transfer function is:

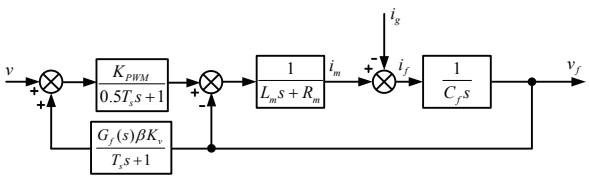

Fig. 4. Block diagram of the equivalent control of a voltage feedforward system.

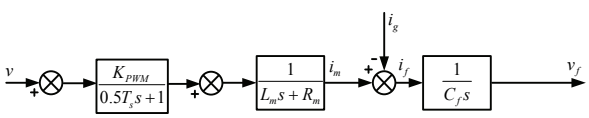

Fig. 5. Block diagram of control after offsetting the voltage feedforward and the physical system feedback.

$$\frac{v_f}{v}=\frac{G_{vsi}(s)G_1(s)G_2(s)}{1+G_1(s)G_2(s)-\beta G_f(s)H_v(s)G_{vsi}(s)G_1(s)G_2(s)} \tag{5}$$

When $\beta=\dfrac{1}{G_f(s)H_v(s)G_{vsi}(s)}$, then：

$$\begin{aligned}\frac{v_f}{v}&=\frac{G_{vsi}(s)G_1(s)G_2(s)}{1+G_1(s)G_2(s)-\beta G_f(s)H_v(s)G_{vsi}(s)G_1(s)G_2(s)}\\&=\frac{G_{vsi}(s)G_1(s)G_2(s)}{1+G_1(s)G_2(s)-G_1(s)G_2(s)}\\&=G_{vsi}(s)G_1(s)G_2(s)\end{aligned} \tag{6}$$

Therefore, by selecting the parameter β, the control block diagram shown in Fig. 5 is obtained. At this time, since the capacitor voltage feedforward and the actual physical system feedback link offset each other, the system reduces two closed loops to simplify the following analysis.

In order to achieve the effect of offset, it usually takes an approximate value of $\beta=1/(K_{PWM}\ H_v)$ in an actual physical system.

For an inductor current feedforward system, the complete elimination of the influence of a load current disturbance on the output voltage is theoretically based on Equation (3). The only required value α is expressed as:

$$\alpha=1+\frac{1}{G_f(s)H_c(s)G_{vsi}(s)G_1(s)G_i(s)} \tag{7}$$

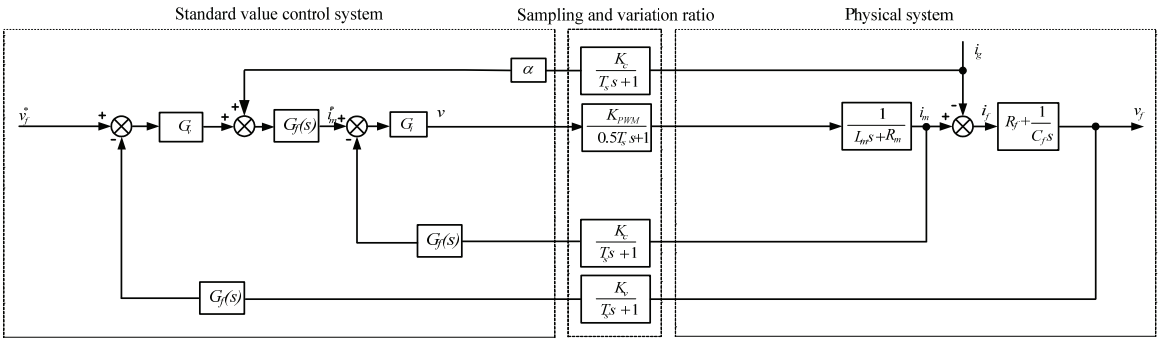

Fig. 6. Block diagram of the VSI double closed-loop control after offsetting the voltage feedforward and physical system feedback.

However, in practice the result is difficult to achieve according to (6). For the sake of simplicity and ease of implementation α=1 is usually taken approximately. Then the control effect amounts to the feedback quantity the current inner loop takes the capacitor current as.

Therefore, according to the above selected feedforward coefficients, it is possible to simplify the control model in the design of a double closed-loop system. For the convenience of analysis, the original five closed-loop system can be simplified as a three closed-loop system. The transfer function $H'_1(s)$ of the simplified voltage gain is:

$$H_1'(s)=\frac{G_f(s)G_{vsi}(s)G_v(s)G_i(s)G_1(s)G_2(s)}{\Delta'(s)} \tag{8}$$

The output impedance transfer function $H'_2(s)$ of the inverter is shown as:

$$H_2'(s)=\frac{G_2(s)(1+G_i(s)G_{vsi}(s)G_1(s)H_c(s)G_f(s))}{\Delta'(s)} -\frac{H_c(s)G_f(s)G_{vsi}(s)G_i(s)G_1(s)G_2(s)}{\Delta'(s)} \tag{9}$$

In the equation,

$$\begin{aligned}\Delta'(s)=&1+G_1(s)G_2(s)\\&+G_f(s)H_c(s)G_{vsi}(s)G_1(s)G_i(s)\\&+G_f^2(s)H_v(s)G_{vsi}(s)G_v(s)G_i(s)G_1(s)G_2(s)\end{aligned} \tag{10}$$

the simplified VSI control block diagram is shown in Fig. 6.

B. Design of Active Damping

In order to increase the voltage stability of the energy storage VSI in the weak grid of an IPS, the preceding output impedance must be lower than the succeeding input impedance in the working frequency range according to the Middlebrook stability impedance criterion. The Nyquist curve of the input/ouput impedance ratio (equivalent loop gain) does not include the point (-1, j0) on the complex plane. Due to the complexity and large disturbances of IPS loads, an increase of the system stability margin needs to reduce the output impedance without changing the voltage characteristics of the VSI to provide a wider range of stable input impedance for the load, which can change some of the unstable working conditions and improve the stability margin.

TABLE I
CALCULATED RESULTS OF THE STABILITY OF AN INVERTER WITH A MOTOR LOAD UNDER DIFFERENT SAMPLING FREQUENCIES

sampling frequency f_s	magnitude margin G_m (dB)	phase margin P_m (deg)	stability
2800	-1.15	3.07	no
3000	-0.836	3.58	no
3200	-0.518	4.15	no
3400	0.432	5.53	yes
3800	0.74	6.14	yes
4000	1.09	6.87	yes

Some studies have shown that the sampling frequency of the inverter influences the output impedance. The higher the sampling frequency, the better the stability. As for the system consisting of an inverter and a three-phase motor load mentioned in Section III-C and Section IV-A, the Nyquist stability criterion is used for the analysis. The results are shown in Table I.

To overcome the oscillatory instability and to obtain a relatively large stability margin, the design method usually adopted in the sampling preservation and variable ratio link is to compress the small time constant which is insuperable as much as possible. However, limited by the actual physical structure of the inverter and the sampling step size, the sampling frequency is not easily improved. To reduce the output impedance of the inverter, this paper uses active damping control to offset the influence of the sampling frequency characteristics. In the VSI double closed-loop control system, a current loop characterized by a fast response is chosen for modification. According to Fig. 6, if the feedback channel, which is composed of the current instruction and filter link, is made equivalent to the forward channel in the loop, a new current inner loop can be obtained, as shown in Fig. 7.

To simplify the analysis, the PI regulator transfer function is written in the zero-pole form:

$$K_{iP}+\frac{K_{iI}}{s}=K_{iP}\frac{\tau_i s+1}{\tau_i s} \tag{11}$$

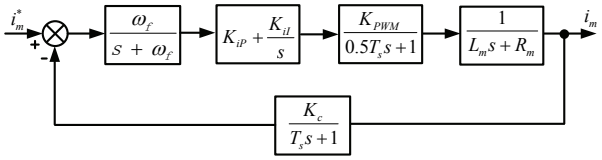

Fig. 7. Structure of the current inner loop.

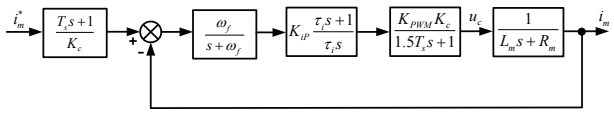

Fig. 8. Simplified structure of the current inner loop.

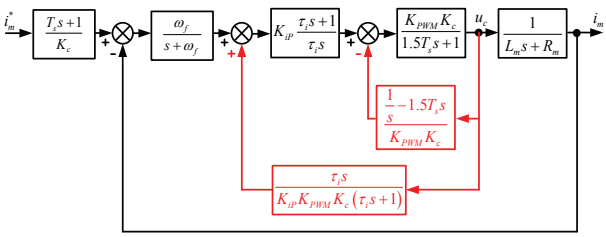

Fig. 9. Control block diagram made by the proposed method.

$$K_{iI}=\frac{K_{iP}}{\tau_i} \tag{12}$$

Since T_s is a small time constant, ignore its higher order term and the combination of the time constants $0.5T_s$ and T_s leads to a simplified current inner loop structure, as shown in Fig. 8.

The sampling frequency characteristic in the current inner loop is $K_{PWM}K_c/(1.5T_s s+1)$. In this loop, two feedback channels are added for compensation. One is the negative feedback added to the voltage u_c of the output end of the PI controller. The other is the positive feedback added to the voltage u_c of the input end. Both of them are used to offset the sampling frequency characteristics. The specific control is shown in Fig. 9.

The modification of the small time constant link is to eliminate T_s in the inner loop by adding two feedback compensations. It is equivalent to a differential link, which can be introduced to improve the system damping and to move the system poles toward the left half plane. As a result, the stability margin can be improved and the system can change from instability to stability. Although the existence of a differential link weakens the high frequency attenuation of a system and generates a resonance peak, this is far higher than the system working frequency band. Therefore, it does not affect the system (as shown in Fig. 12(a)). On the other hand, the traditional active damping control method makes the order of the feedback channel transfer function higher, since using two feedback channel offset small time constants instead of the traditional active damping control is easier to implement in practice.

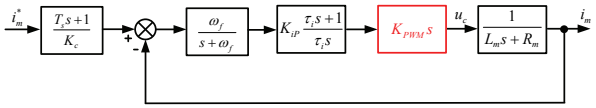

Fig. 10. Equivalent current loop structure.

After adding two feedback compensations to the control system in Fig. 9, its block diagram is shown in Fig. 10.

For the voltage outer loop, the traditional voltage outer loop control is used. The control block diagram is shown in Fig. 11.

Suppose $G'_{vsi}(s)=K_{PWM}s$. It is then possible to obtain the following expressions for the voltage gain transfer function $H_{eq1}(s)$ and the output impedance transfer function $H_{eq2}(s)$ of the VSI active damping control based on virtual compensation.

$$H_{eq1}(s)=\frac{G_f(s)G'_{vsi}(s)G_v(s)G_i(s)G_1(s)G_2(s)}{\Delta'(s)} \tag{13}$$

$$H_{eq2}(s)=\frac{G_2(s)(1+G_i(s)G'_{vsi}(s)G_1(s)H_c(s)G_f(s))}{\Delta'(s)} -\frac{H_c(s)G_f(s)G'_{vsi}(s)G_i(s)G_1(s)G_2(s)}{\Delta'(s)} \tag{14}$$

C. Analysis of Effect

The voltage gain transfer function and the output impedance transfer function are compared for the conventional voltage source double closed-loop control and the proposed active damping control based on virtual compensation. According to the equivalent loop gain Nyquist curve of the Middlebrook impedance criterion, the stability of the system is analyzed.

The parameters are selected as L_m=190μH, L_g=55μH, R_m=0.6mΩ, R_g=0.6mΩ, C_f=300μF, f_s=3200Hz, and $K_{PWM}=650/\sqrt{3}$. V_{base}=390/1.732*1.414, so that the voltage sampling ratio $K_v=1/V_{base}$=1/318; I_{base}=703*1.414, so that the current sampling ratio $K_c=1/I_{base}$=1/994; K_{vP} and K_{vI} are the P parameter and I parameter of the PI controller in the voltage outer loop, K_{vP}=1.0249, $K_{vI}=0.0065/T_s$, K_{iP} and K_{iI} are the P parameter and I parameter of the PI controller in the current inner loop, and K_{iP}=0.5367 and $K_{iI}=0.0254/T_s$. Their values are set according to the control parameters of the inverter in the laboratory to ensure the best control effect. The system transfer function bode diagram is shown in Fig. 12.

According to Fig. 12(a), the sampling frequency link is converted into a pure differential link though feedback compensation, with the result that the high frequency attenuation of the system become weak and a resonance peak appears. However, this is a lot higher than the system working frequency band. Therefore, the system is not affected. In the working frequency range, the voltage gain transfer function of the system is basically consistent in terms of magnitude and property. According to Fig. 12(b), a significant decrease in the output impedance of the system in

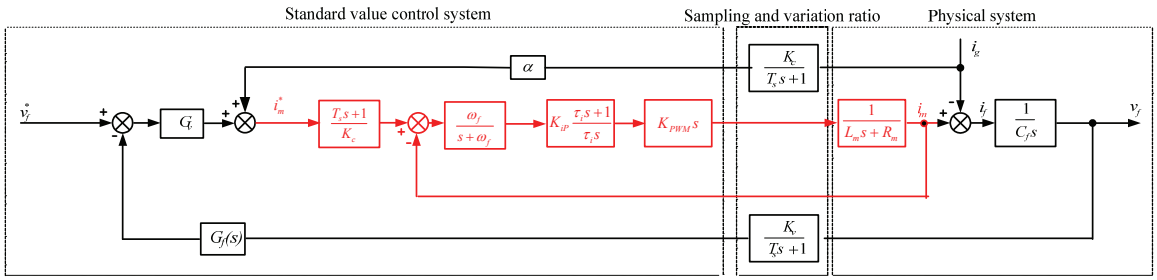

Fig. 11. Equivalent control block diagram of a VSI made by the proposed method.

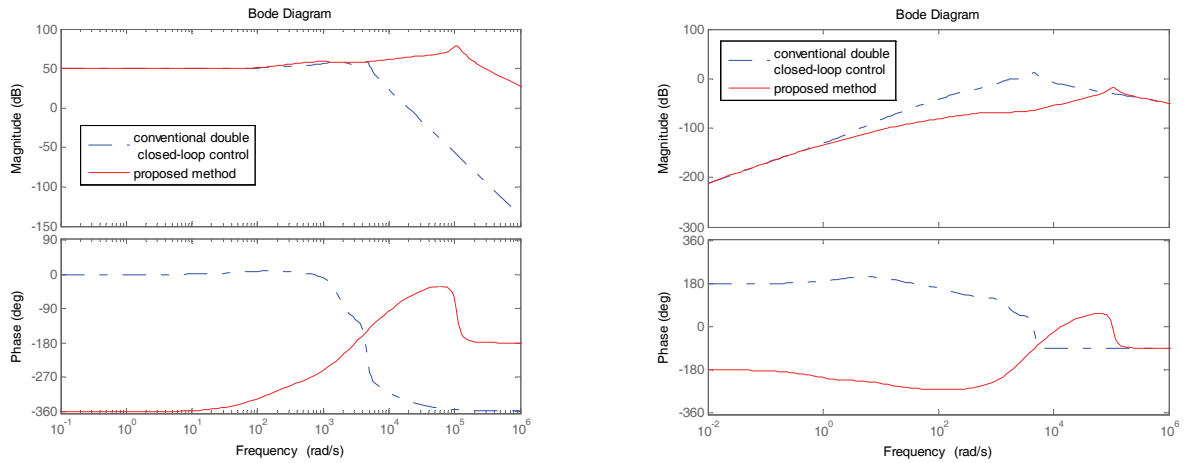

(a) (b)

Fig. 12. Comparison of the proposed method with the conventional method: (a) Bode diagram of the voltage gain transfer function; (b) Bode diagram of the output impedance transfer function.

the range of the working frequency leads to a broadening of the input impedance range of the system load and an increase in the stability margin of the system.

IV. Analysis of Examples

A. Frequency Domain Analysis

A Nyquist curve of the equivalent loop gain is used to analyze the change of the system stability caused by the proposed method. With the three-phase motor taken as a load, its stator and rotor resistances are R_s and R_r, its stator and rotor leakage reactances are X_s and X_r, its excitation reactance is X_m, its actual angular velocity is ω_m, and its synchronous angular velocity is ω_s. According to its mathematical model and without consideration of the rotor motion equation, the input admittance matrix $\boldsymbol{Y}$ of its load can be expressed as:

$$\boldsymbol{Y}=\left[R_{\mathrm{s}}\cdot\boldsymbol{I}_2+\boldsymbol{A}-\boldsymbol{B}\cdot\left(R_{\mathrm{r}}\cdot\boldsymbol{I}_2+\boldsymbol{D}\right)^{-1}\cdot\boldsymbol{C}\right]^{-1} \tag{15}$$

In this equation, each matrix satisfies:

$$\boldsymbol{A}=(X_{\mathrm{s}}+X_{\mathrm{m}})\cdot\begin{bmatrix}s & -\omega_{\mathrm{s}}\\ \omega_{\mathrm{s}} & s\end{bmatrix},\quad \boldsymbol{B}=X_{\mathrm{m}}\cdot\begin{bmatrix}s & -\omega_{\mathrm{s}}\\ \omega_{\mathrm{s}} & s\end{bmatrix},$$

$$\boldsymbol{C}=X_{\mathrm{m}}\cdot\begin{bmatrix}s & -(\omega_{\mathrm{s}}-\omega_{\mathrm{m}})\\ \omega_{\mathrm{s}}-\omega_{\mathrm{m}} & s\end{bmatrix},$$

$$\boldsymbol{D}=(X_{\mathrm{r}}+X_{\mathrm{m}})\cdot\begin{bmatrix}s & -(\omega_{\mathrm{s}}-\omega_{\mathrm{m}})\\ \omega_{\mathrm{s}}-\omega_{\mathrm{m}} & s\end{bmatrix}$$

Where $s=j\omega$ is the frequency domain operator. Since $\boldsymbol{A}$, $\boldsymbol{B}$, $\boldsymbol{C}$ and $\boldsymbol{D}$ are normal matrices, $\boldsymbol{Y}(s)$ is a symmetric matrix:

$$\boldsymbol{Y}_L(s)=\begin{bmatrix}Y_{\mathrm{Ldd}}(s) & Y_{\mathrm{Ldq}}(s)\\ -Y_{\mathrm{Ldq}}(s) & Y_{\mathrm{Ldd}}(s)\end{bmatrix} \tag{16}$$

The equivalent input impedance Z_L of the motor satisfies:

$$Z_L(s)=\frac{1}{2\left\|\boldsymbol{Y}_L(s)\right\|_1}=\frac{1}{2\max\left\{\left|Y_{Ldd}\right|+\left|Y_{Lqd}\right|,\left|Y_{Ldq}\right|+\left|Y_{Lqq}\right|\right\}} \tag{17}$$

Then the load parameters of the three-phase motor are chosen as R_s=0.0687, R_r=0.0604, X_s=0.0001, X_r=0.0001, X_m=0.0151, ω_m=0.995ω_s, ω_s=100π, P_L=90kW, and u_L=380V. A Nyquist curve of the equivalent loop gain $T_m=Z_o/Z_L$ is shown as follows:

As show in Fig. 13, a Nyquist curve of the equivalent loop gain T_m on the plane of s under the conventional double closed-loop control surrounded the point (-1, j0), where it is possible to judge that the system under that control is unstable. By use of the virtual compensation active damping control proposed in this paper, a Nyquist curve of the equivalent loop gain T_m on the plane of s does not surrounded

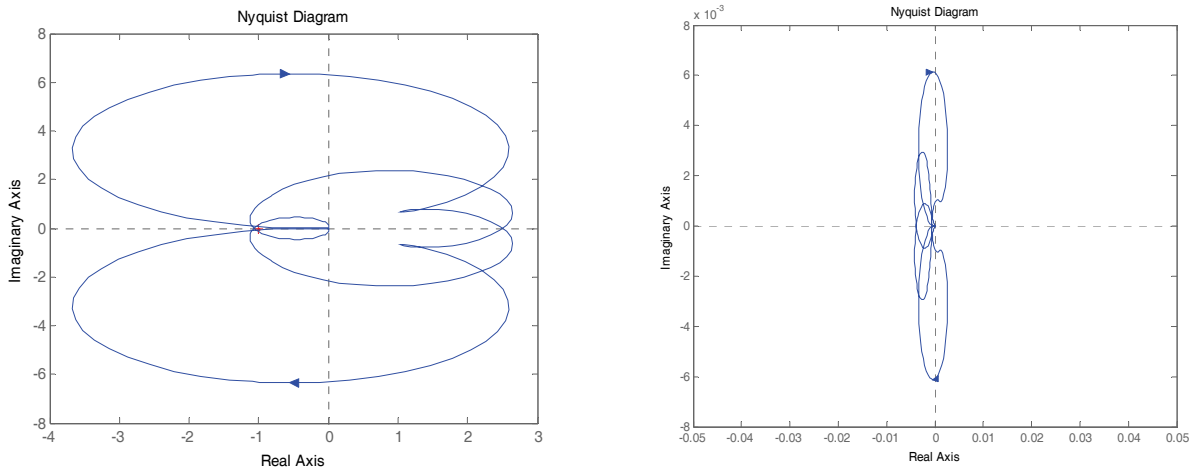

(a) (b)

Fig. 13. Comparison of the Nyquist curves of T_m by the conventional method and the proposed method: (a) Conventional Double closed-loop control; (b) Proposed method.

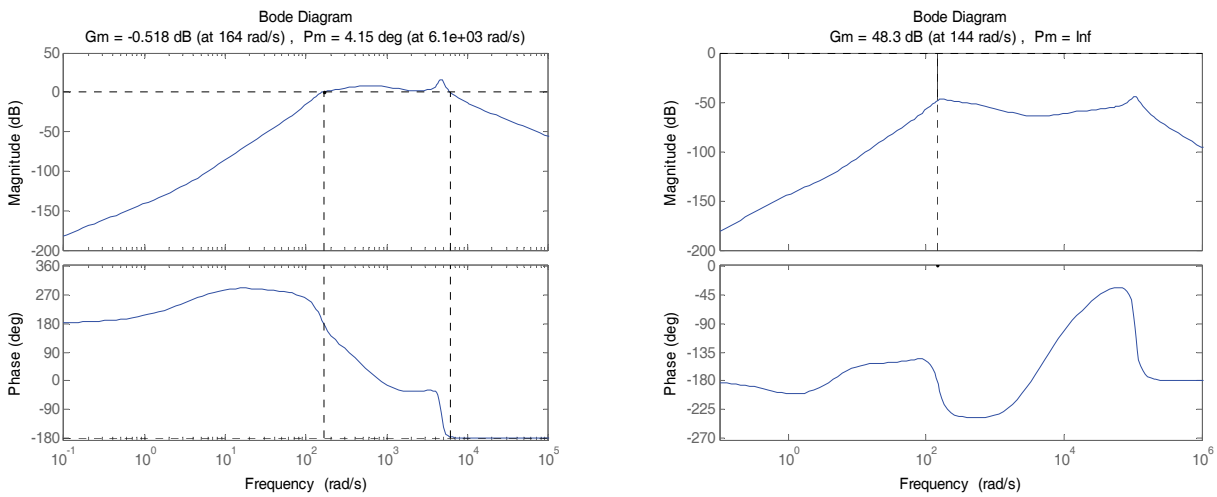

(a) (b)

Fig. 14. Stability margin using the conventional method and the proposed method: (a) Conventional double closed-loop control; (b) Proposed method.

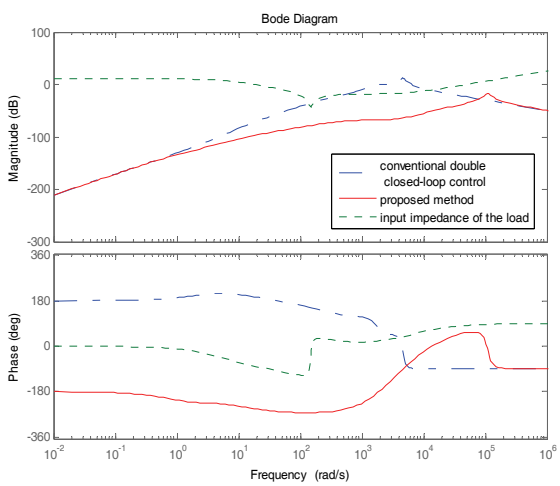

Fig. 15. Bode diagram of the output impedance and the input impedance.

(-1, j0). Therefore, the system changes from instability to stability.

Fig. 14 shows the stability margin of a VSI using the conventional double closed-loop control and the proposed method. The gain margin of the conventional double closed-loop system is Gm=-0.518 dB, which represents the instability of the system. The gain margin using the proposed method is Gm=48.3 dB, which represents an increase in the stability margin of the system and a change from instability to stability.

From Fig. 15 it is shown that the output impedance curve of the conventional double closed-loop control intersects with the input impedance curve of the load, and that the output impedance curve of the proposed method does not intersect with the input impedance curve of the load. This shows that the proposed method can improve the system stability and broaden the range of stable operation.

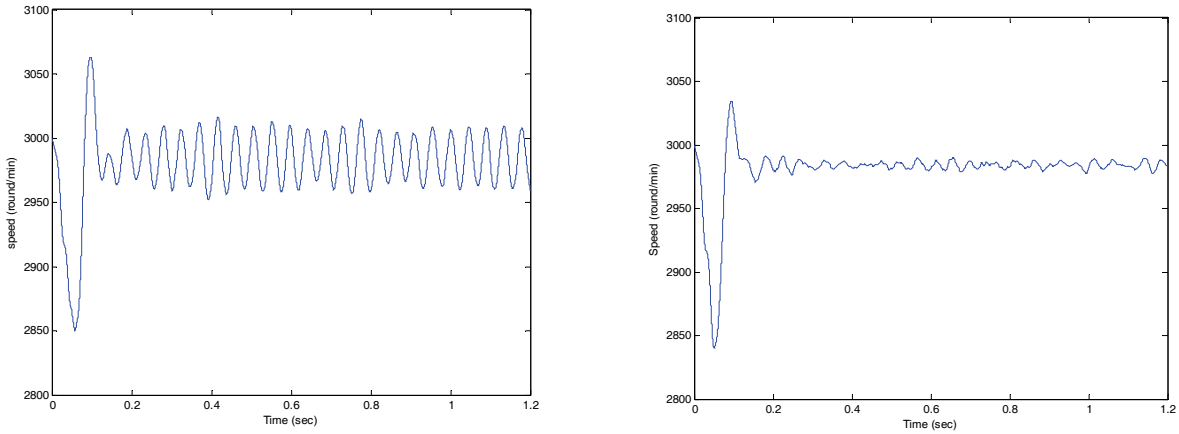

(a) (b)

Fig. 16. Motor load speed using the conventional method and the proposed method: (a) Conventional double closed-loop control; (b) Proposed method.

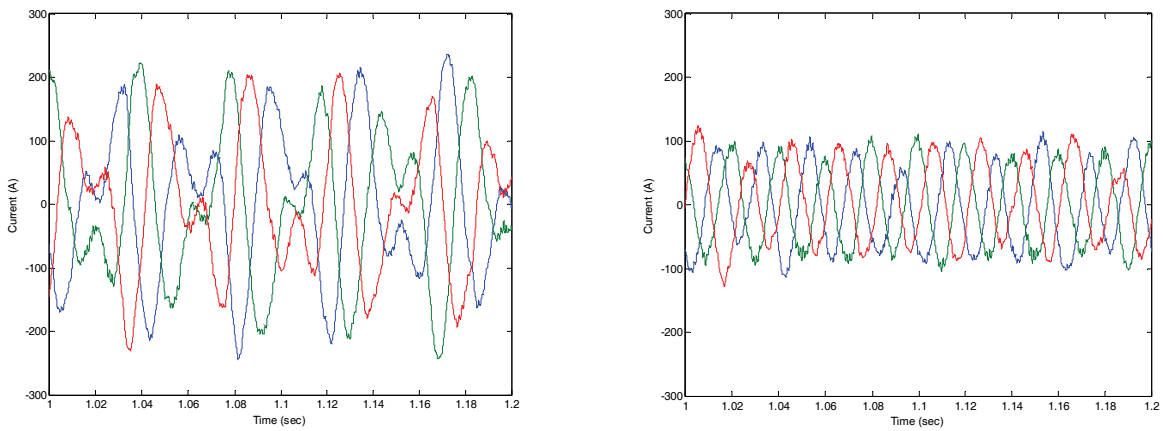

(a) (b)

Fig. 17. Inverter output current waveforms using the conventional method and the proposed method: (a) Conventional double closed-loop control; (b) Proposed method.

B. Simulation Analysis

A simulation model of a double closed-loop control VSI with a three-phase motor load is established in MATLAB/ Simulink. According to Fig. 9, the voltage u_c is taken as a feedback quantity, which is used to modify the current loop through double feedback compensation. Fig. 16 to Fig. 18 give a comparison between the simulation waveform load torques T_L=74Nm (25% rated power output) of the motor when the two method are adopted.

It can be seen from Fig. 16 that the system oscillates and cannot run stably when the VSI uses the conventional double closed-loop control for a motor load with the given parameters. If the proposed method is adopted for controlling the inverter, the system is restored to stability. As shown in Fig. 17, the application of the proposed method leads a significant improvement on the current waveform stability. Because the Middlebrook impedance stability criterion is conservative, when it is only Z_{soure}/Z_{load} <1, and the selected unstable conditions are quite extreme, the system current does not perform well even though it is stable. However, the proposed method improved the stability and stability margin of the system by reducing the output impedance of the source. Fig. 18 shows that the use of the conventional control makes the amplitude of the voltage waveform continuously change, while the adoption of the proposed method causes it to be stable.

C. Experimental Verification

In order to verify the method proposed in this paper, an experimental system is set up in the laboratory, as shown in Fig. 19. A photograph of the experimental setup is shown in Fig. 20.

The energy storage power source is replaced by a 700V dc which is obtained from the conversion of a 380V electric supply via the three phase rectifier and serves as the VSI input voltage. The rated capacity of the VSI is 30kVA. The 700V dc power is converted into a 380V ac power, which is then connected to the motor load node by an isolating transformer T. The motor load is 10kW. Since a power

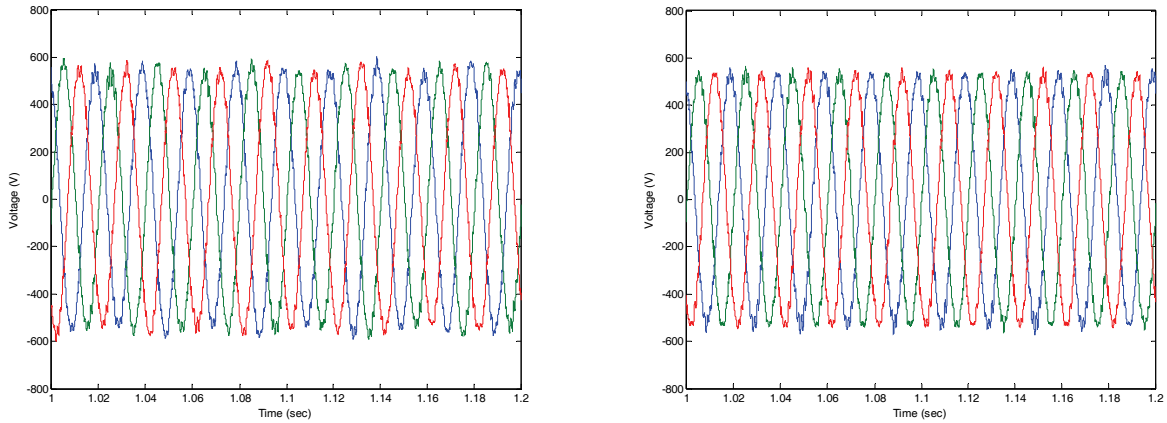

(a) (b)

Fig. 18. Inverter output voltage waveforms using the conventional method and the proposed method: (a) Conventional double closed-loop control; (b) Proposed method.

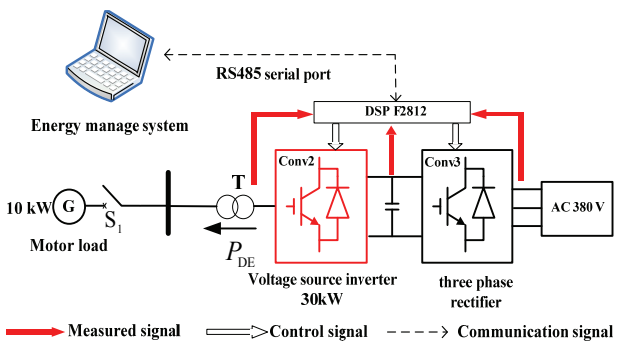

Fig. 19. Structure of the experimental system.

Fig. 20. Photograph of the experimental system.

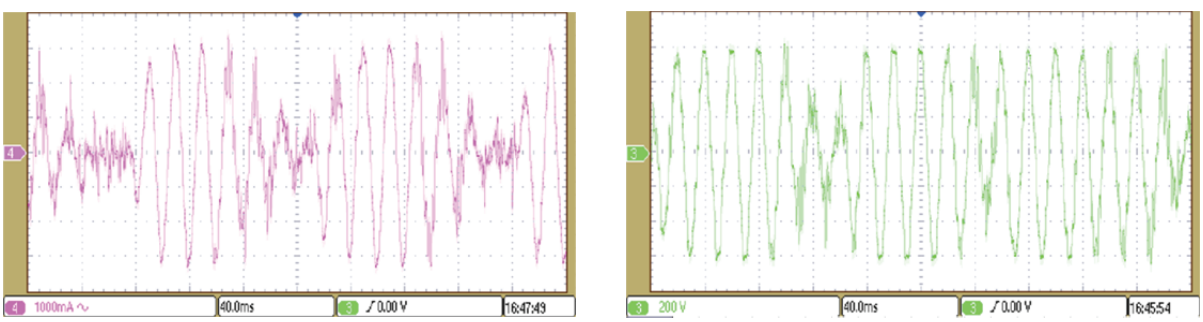

(a) (b)

Fig. 21. Inverter using the conventional double closed-loop control: (a) Waveform of the output current; (b) Waveform of the output voltage.

electronic device is adopted as a source, the short circuit capacity of the system is not large due to the current-limiting of the voltage source inverter. Therefore, the ratio of the system short circuit capacity to the system rated capacity is not large, As a result, the system presents the characteristics of a weak grid. In the experimental platform, the control chip of both the rectifier and the inverter is a DSP F2812. The controller carries out real-time data transmission with a computer through a RS485 serial port. The waveforms of voltage, current and power are collected through the RS485 serial port. In order to verify the proposed method, this paper designs an experimental process where the conventional VSI double closed-loop control and the active damping control with additional virtual compensation are used to carry out experiments on the 30kVA VSI with a motor in a light-load state (20% motor rated power).

Fig. 21 shows output current and voltage waveforms of the inverter in using the conventional double closed-loop control. Fig. 22 shows output current and voltage waveforms of the inverter in using the proposed method.

A comparative analysis of the experimental waveforms shows that the proposed method can be used to change the

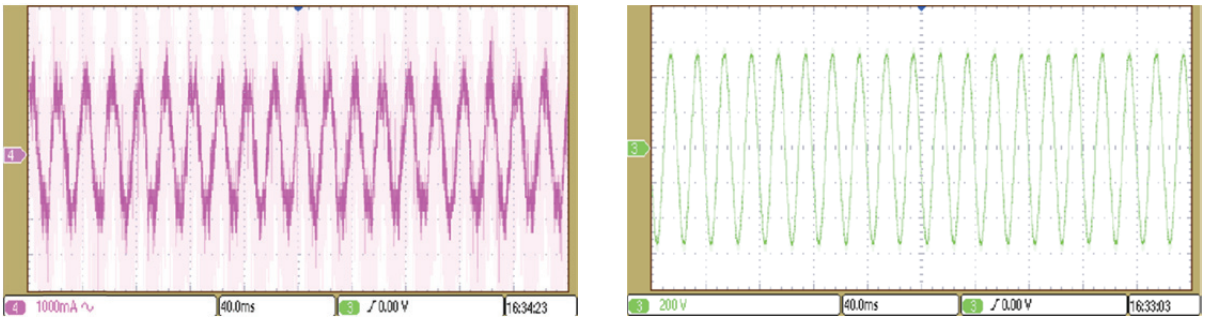

(a) (b)

Fig. 22. Inverter using the proposed control: (a) Waveform of the output current; (b) Waveform of the output voltage.

system from instability to stability and to broaden its range of stable operation. The proposed method is shown to be both feasible and effective.

V. Conclusion

In order to extend the range of the allowable load input impedance under stable operation, this paper proposed a VSI active damping control based on virtual compensation. This control is used to offset the sampling frequency characteristic by introducing a virtual compensation feedback into the current inner loop. Thus, it can reduce the output impedance of the VSI, and improve the stability of the system. Simulations and experiments verify that the proposed method is both feasible and effective.

Acknowledgment

This work was supported in part by the National Natural Science Foundation of China (51607184 and 51607185), and 973 project (613294).

References

[1] D. Yang, X. Wang, F. Liu, K. Xin, Y. Liu, and F. Blaabjerg, "Adaptive reactive power control of PV power plants for improved power transfer capability under ultra-weak grid conditions," *IEEE Trans. Smart Grid*, to be published.

[2] T. Stetz, F. Marten, and M. Braun, "Improved low voltage grid-integration of photovoltaic systems in germany," *IEEE Trans. Sustain. Energy*, Vol. 4, No. 2, pp. 534-542, Apr. 2013.

[3] J. Wang, J. Yao, H. Hu, Y. Xing, X. He, and Kai Sun, "Impedance-based stability analysis of single-phase inverter connected to weak grid with voltage feed-forward control," in *Proc. IEEE APEC*, pp. 2182-2186, 2016.

[4] X. Li, X. Wu, Y. Geng, X. Yuan, C. Xia, and X. Zhang, "Wide damping region for LCL-type grid-connected inverter with an improved capacitor-current-feedback method," *IEEE Trans. Power Electron.*, Vol. 30, No. 9, pp. 5247-5259, Sep. 2015.

[5] J. Xu, S. Xie, B. Zhang, and Q. Qian, "Robust grid current control with impedance-phase shaping for LCL-filtered inverters in weak and distorted grid," *IEEE Trans. Power Electron.*, Vol. 33, No. 12, pp. 10240-10250, Dec. 2018.

[6] L. Jia, X. Ruan, W. Zhao, Z. Lin, and X. Wang, "An adaptive active damper for improving the stability of grid-connected inverters under weak grid," *IEEE Trans. Power Electron.*, Vol. 33, No. 11, pp. 9561-9574. Nov. 2018.

[7] C. A. Busada, S. G. Jorge, and J. A. Solsona, "Full-state feedback equivalent controller for active damping in, *LCL*-filtered grid-connected inverters using a reduced number of sensors," *IEEE Trans. Ind. Electron.*, Vol. 62, No. 10, pp. 5993-6002, Oct. 2015.

[8] Y. Geng, Y. Yun, R. Chen, K. Wang, H. Bai, and X. Wu, "Parameters design and optimization for lc-type off-grid inverter with inductor-current-feedback active-damping," *IEEE Trans. Power Electron.*, Vol. 33, No. 1, pp. 703-715. Jan. 2018.

[9] A. Riccobono and E. Santi, "Positive feedforward control of three-phase voltage source inverter for DC input bus stabilization with experimental validation," *IEEE Tran. Ind. Appl.*, Vol. 49, No. 1, pp. 168-177, Jan. 2013.

[10] J. W. Jung, N. T.-T. Vu, D. Q. Dang, T. D. Do, Y.-S Choi, and H. H. Choi, "A three-phase inverter for a standalone distributed generation system: Adaptive voltage control design and stability analysis," *IEEE Trans. Energy Convers.*, Vol. 29, No. 1, pp.46-56, Mar. 2014.

[11] S. Eren, M. Pahlevaninezhad, A. Bakhshai, and P. K. Jain, "Composite nonlinear feedback control and stability analysis of a grid-connected voltage source inverter with LCL filter," *IEEE Trans. Ind. Electron.*, Vol. 60, No. 11, pp.5059-5074, Nov. 2013.

[12] S. Eren, M. Pahlevaninezhad, A. Bakhshai, and P. Jain, "An adaptive droop DC-bus voltage controller for a grid-connected voltage source inverter with LCL filter,". *IEEE Trans. Power Electronics*, Vol. 30, No. 2, pp. 547-560, Feb. 2015.

[13] S. Yang, Q. Lei, F. Z. Peng, and Z. Qian, "A robust control scheme for grid-connected voltage-source inverters," *IEEE Trans. Ind. Electron.*, Vol. 58, No. 1, pp. 202-212, Jan. 2011.

[14] H. Wang, L. Fu, F. Xiao, G. Jie, and W. Zhu, "A double-loop control strategy for three-phase inverter with unbalanced load," *Power Syst. Technol.*, Vol. 37, No. 2, pp. 398-404, Feb. 2013.

Jian Hu received his B.S. degree in Automation from the Beijing Institute of Technology, Beijing, China, in 2012; and his M.S. degree in Control Science and Engineering from the Naval University of Engineering, Wuhan, China, in 2014, where he is presently working towards his Ph.D. degree in Electrical Engineering at the National Key Laboratory of Science and Technology on Vessel Integrated Power Systems. His current research interests include power system stability analysis and control.

Lijun Fu received his B.S. degree in Electrical Engineering from the Hunan University of Science and Technology, Xiangtan, China, in 1989; and his M.S. and Ph.D. degrees from Wuhan University, Wuhan, China, in 1995 and 1997, respectively. He is presently working as a Professor in the National Key Laboratory of Science and Technology on Vessel Integrated Power Systems, Naval University of Engineering, Wuhan, China. His current research interests include power system design and simulation modeling.